



ELSEVIER

Available online at www.sciencedirect.com

ScienceDirect

journal homepage: www.elsevier.com/locate/he

The kinetics of acetic acid steam reforming on Ni/Ca-Al₂O₃ catalyst

Jennifer Reeve^a, Tariq Mahmud^a, Martyn V. Twigg^b, Valerie Dupont^{a,*}

^a School of Chemical and Process Engineering, The University of Leeds, Leeds, LS2 9JT, UK

^b Twigg Scientific and Technical Limited, Cambridge, CB23 3PQ, UK

HIGHLIGHTS

- Kinetics of acetic acid (AcOH) steam reforming over Ni/Ca-Al₂O₃ catalyst.
- Negligible carbon deposition and no mass transfer limitations are demonstrated.
- Kinetic parameters derived for four models of 3–5 reactions fitted using gPROMS.
- Excellent fit obtained for model with SR AcOH, AcOH decomposition, and WGS.
- Validation for temperature (600–700 °C) and steam to carbon ratio (3–6) at 1 atm.

ARTICLE INFO

Article history:

Received 30 May 2022

Received in revised form

11 August 2022

Accepted 16 August 2022

Available online 21 September 2022

Keywords:

Kinetics

Modelling

Acetic acid

Steam reforming

Nickel

Packed bed

ABSTRACT

As a significant by-product of many thermochemical and biological waste conversion processes, acetic acid (AcOH) is often investigated as model feedstock in the production of sustainable hydrogen from non-fossil sources. The kinetics of its steam reforming were extracted from packed bed reactor experiments over an industrially produced 14 wt% Ni/Ca-Al₂O₃ catalyst at atmospheric pressure. The model consisting of AcOH steam reforming producing CO₂ and H₂, AcOH decomposition to CO and H₂, and water gas shift, achieved the best fit, reflected in the lowest average relative errors (ARE) with experimental results, with ARE values below 5.4% and 6.4% on AcOH and water conversions respectively, and below 4% on H₂ mol fraction. This model was validated away from equilibrium using additional experimental points, as well as for a wide range of equilibrium conditions with varying temperature (600–700 °C) and feed molar steam to carbon ratios (3–8) at atmospheric pressure using an independent method.

© 2022 The Author(s). Published by Elsevier Ltd on behalf of Hydrogen Energy Publications LLC. This is an open access article under the CC BY license (<http://creativecommons.org/licenses/by/4.0/>).

Introduction

Biomass derived wastes are collectively considered to be increasingly viable sustainable alternative resources in the production of green gases, where the latter can play an important role in decarbonising the heat, power and transport

sectors through injection in the gas distribution grid, hydro-treating at refineries and biorefineries, Fischer-Tropsch synthesis of liquid fuels, and fuel cells.

The following biomass conversion processes all share the generation of significant amounts of acetic acid while providing essential waste treatment: fast pyrolysis of lignocellulosic biomass wastes [1–5], gasification of humin [6],

* Corresponding author. School of Chemical and Process Engineering, The University of Leeds, Leeds, LS2 9JT, UK.

E-mail address: V.Dupont@leeds.ac.uk (V. Dupont).

<https://doi.org/10.1016/j.ijhydene.2022.08.167>

0360-3199/© 2022 The Author(s). Published by Elsevier Ltd on behalf of Hydrogen Energy Publications LLC. This is an open access article under the CC BY license (<http://creativecommons.org/licenses/by/4.0/>).

hydrothermal carbonisation of lignocellulosic wastes [7], as well as fermentation routes like the acidogenesis and acetogenesis stages from the anaerobic digestion of carbohydrate-rich substrates [8]. A number of studies have therefore proposed acetic acid ('AcOH') as model compound for steam reforming [9–12] and other advanced reforming processes for the production of hydrogen [13,14], syngas [15] and synthetic natural gas (SNG) [16], as a first step in building a design capability of reforming realistic mixtures of bio-compounds. A key requirement in achieving credible designs of these strategically important processes is the use of kinetic rates for the individual steps involved in the reforming processes.

Due to its comparatively low cost, global availability, and high activity in the C-C and C-O bonds cleavage, the oxidative conversion of methane, as well as CO₂ and H₂O reforming [17], nickel continues to dominate the market of oxidative reforming catalysts. Routes to recycle these catalysts have been established in industry [18]. Unlike other elements put forward for advanced reforming, such as platinum group metals, cobalt, or rare earth metals, nickel does not appear in the EU list of critical raw materials [19,20] and was only recently added in that of the United States' Geological Survey's list of critical minerals [21]. In addition, Ni is frequently used in chemical looping reforming due to its ease of reduction-oxidation [22] and its ability to act simultaneously as oxygen transfer material and reforming catalyst [23]. Doping the catalyst support with low-cost alkaline earth metals (Ca, Mg, Ce) has long been known to reduce acidity of the catalyst and its support, thus inhibiting the formation of coke during nickel based catalytic reforming [15,24]. Ca is claimed to also improve dispersion of the active phase on ceramic supports, thereby preventing the sintering of active metal phase in Ni catalysed reforming environments [25–28], and promoting water adsorption [29]. Kinetic data on the steam reforming reactions of significant bio-compounds is currently lacking, which limits the ability to develop reliable models for the design of advanced reforming processes of bio-feedstock. In order to help address this gap, the present study aims to derive kinetic data for acetic acid on a Ni supported CaO-Al₂O₃ catalyst prepared using industrial methods by Twig Scientific and Technical Ltd.

Various experimental studies have examined acetic acid steam reforming [13,23,30–35], as it is one of the most abundant compounds in pyrolysis bio-oil [36–39]. In order to carry out the kinetic study, it was also useful to review existing knowledge of reaction pathways. When acetic acid undergoes steam reforming, the reaction scheme is complex, with multiple possible side reactions. A summary of the key reactions is given in Table 1.

Of these reactions, ketonization (6) and dehydration to ketene (7) result in products which are precursors to coke formation [36]. Ketonization is particularly prominent at lower temperatures, or in the presence of acidic sites, such as Al₂O₃ [35,41,42]. Several authors have attempted to describe the reaction pathways in greater detail. In 1996, Wang et al. [43] proposed a mechanism for the steam reforming reaction on Ni-based catalysts, in which the acetic acid forms adsorbed acetate species that decompose to form CO₂ and H₂. Trane et al. [36] proposed that the elementary steps for these reactions would be similar to those that occur during steam methane reforming. Reaction mechanisms have since been

Table 1 – Summary of reactions in steam reforming of acetic acid [36,40].

Main reactions		
R1	SR acetic acid	$\text{CH}_3\text{COOH} + 2\text{H}_2\text{O} \rightarrow 2\text{CO}_2 + 4\text{H}_2$
R2	Decomposition 1	$\text{CH}_3\text{COOH} \rightarrow 2\text{H}_2 + 2\text{CO}$
R3	Decomposition 2	$\text{CH}_3\text{COOH} \rightarrow \text{CH}_4 + \text{CO}_2$
R4	SMR	$\text{CH}_4 + \text{H}_2\text{O} \leftrightarrow \text{CO} + 3\text{H}_2$
R5	Water gas shift	$\text{CO} + \text{H}_2\text{O} \leftrightarrow \text{H}_2 + \text{CO}_2$
R6	Ketonization	$2\text{CH}_3\text{COOH} \rightarrow \text{CH}_3\text{COCH}_3 + \text{CO}_2 + \text{H}_2\text{O}$
R7	Dehydration	$\text{CH}_3\text{COOH} \rightarrow \text{CH}_2\text{CO} + \text{H}_2\text{O}$
Secondary reactions		
R8	SR acetone	$\text{CH}_3\text{COCH}_3 + 3\text{H}_2\text{O} \rightarrow 3\text{CO} + 6\text{H}_2$
R9	SR ketene	$\text{CH}_2\text{CO} + \text{H}_2\text{O} \rightarrow 2\text{CO} + 2\text{H}_2$
R10	Ketene coupling	$2\text{CH}_2\text{CO} \rightarrow \text{C}_2\text{H}_4 + 2\text{CO}$
R11	Acetone 1	$2\text{CH}_3\text{COCH}_3 \rightarrow \text{H}_2\text{O} + (\text{CH}_3)_2\text{CCHCOCH}_3$
R12	Acetone 2	$(\text{CH}_3)_2\text{CCHCOCH}_3 + \text{CH}_3\text{COCH}_3 \rightarrow \text{C}_9\text{H}_{12} + 2\text{H}_2\text{O}$
R13	Acetone 3	$\text{C}_9\text{H}_{12} \rightarrow \text{coke}$

proposed for various other catalysts. For example, Lemonidou et al. [35] examined the reaction pathway on Rh supported on La₂O₃/CeO₂-ZrO₂, Takanabe et al. [44] proposed a pathway for Pt/ZrO₂ catalysts, and Wang et al. [45] examined the mechanism on Co-Fe catalysts. Resende et al. [41] examined steam reforming on a LaNiO₃ perovskite-type catalyst, with similarities to the mechanism proposed by Wang et al. [43]. Hoang [46] reviewed several papers in order to produce a generalized reaction pathway, in which acetic acid decomposes to H₂, coke and CO, some of which is converted by WGS. Megia et al. [47] derived a kinetic model consisting of four global reactions for acetic acid steam reforming on cobalt based catalysts between 500 and 600 °C at S/C of 2, in which ketone and methane were intermediates and potentially significant by-products. In [48] and using ceria-zirconia supports, Phongprueksathat et al. identify differences of mechanisms pathways between Ni and Co catalysed steam reforming of acetic acid. They concluded that above 550 °C and for S/C of 3–9, Ni favoured the steam reforming route without acetone or CH₄ in the products resulting in higher H₂ yield, and consistent with equilibrium predictions, which they attribute to higher C-C bond cleavage activity. In contrast, Co and the support itself promoted the ketonization route to acetone which could result in carbon deposition.

The following study aims to propose a kinetic model for acetic acid steam reforming, Using a simplified reaction scheme, based on the above literature review. Kinetic parameters are estimated by fitting the models to experimental measurements.

Methodology

Experimental methodology

The reactor set-up and operating procedure are outlined below. Acetic acid steam reforming was carried out in the packed bed reactor set-up illustrated in Fig. 1.

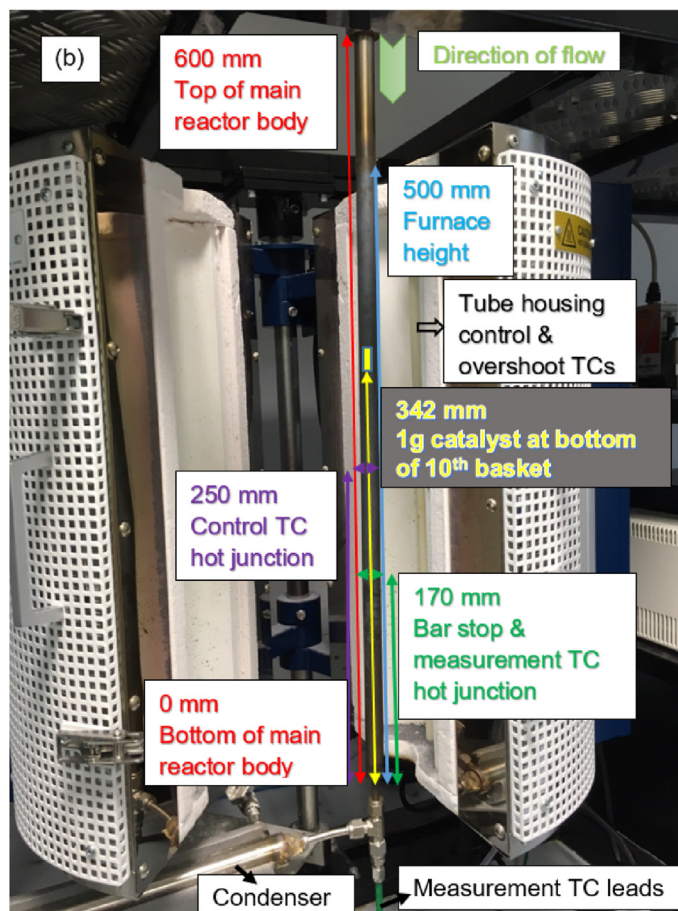
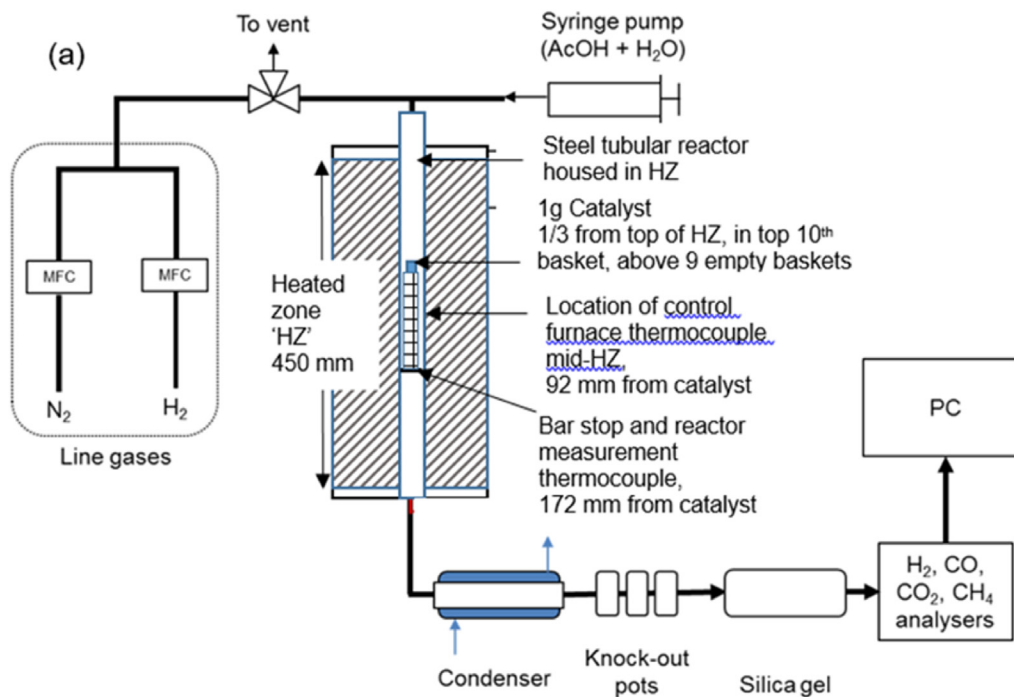


Fig. 1 – (a) Reactor set-up for acetic acid steam reforming experiments, (b) dimensions of reactor and furnace, and locations of catalyst and thermocouples.

Table 2 – Experimental conditions used for kinetic study.

Design/operating parameter	Value		
Catalyst	18 wt% NiO/Calcium Aluminate		
Catalyst diameter (μm)	150–250		
Outlet pressure (bar)	1.01325		
Temperature ($^{\circ}\text{C}$)	550	620	650
S/C ratio (–)	3	3.5	4
Feed mole fraction (–)	AcOH	H ₂ O	N ₂
	0.048	0.342	0.610
	0.058	0.342	0.6
	0.058	0.410	0.531
	0.058	0.473	0.469
Feed volumetric flow rate at STP ($\text{cm}^3 \text{min}^{-1}$)	AcOH + H ₂ O solution	N ₂	
	0.109–0.921	150–800	

Methodologies for the characterisation of the catalyst are provided in an earlier publication where it is named catalyst 'B' [14]. To summarise, MBET surface area of the fresh (fully oxidised catalyst) was $34.9 \text{ m}^2 \text{ g}^{-1}$, pore volume $0.068 \text{ cm}^3 \text{ g}^{-1}$ and pore radius 1.9 nm. The support is expected to present a molar Ca to Al ratio of 5 comprised of CaO and Al₂O₃, the fresh catalyst has 18 wt% NiO (14.1 wt% Ni) as described in [29].

The reactor was a 316 stainless steel tube, 750 mm long, with a main reactor body (section with largest constant diameter) that was 600 mm long with an inside diameter of 13.2 mm. The main reactor body was placed within an Elite Thermal Systems vertical furnace (TSVH12/30/450) with 1.7 kW electrical input, featuring a 450 mm isothermal heated zone ('HZ') ensured by high grade resistance wire spirals, fitted with a Eurotherm 3216 temperature controller, whose control thermocouple was located in ceramic tube half way down the HZ and almost touching the reactor. To enable monitoring of the reaction temperature, a K-type thermocouple was also placed inside the reactor (more on this later). To minimise heat losses, gaps at the top and base of the reactor were covered with thermal insulation (Superwool® 607 HT paper). A solution of AcOH and deionised H₂O, mixed to the required S/C ratio, was fed from a programmable New Era syringe pump. The rig was also connected to a supply of N₂ and H₂ (BOC, purity 99.995%) for the pre-reduction step of the catalyst. A Bronkhorst MASS-VIEW mass flow controller (0–2000 sccm) controlled the flow of N₂, while a Bronkhorst EL-FLOW (0.1–200 sccm) controlled H₂ flow. After catalyst pre-reduction in H₂, the MBET surface was $28.8 \text{ m}^2 \text{ g}^{-1}$, pore volume and radius increased to $0.114 \text{ cm}^3 \text{ g}^{-1}$ and 2.4 nm. A catalyst bed was created by placing 1g of fresh, oxidised catalyst (from large catalyst pellets ground to particle size 150–250 μm using a pestle and mortar), whose properties are given in Table 2 and Table 3, into a cylindrical stainless steel mesh basket (1250 mm^3 , 9.1 mm ID, 19.1 mm H). The catalyst filled half the volume of a basket, thus consisting in a plug 9 mm high. In this set up that allowed 10 different locations for the catalyst along the reactor, the most stable time on stream concentrations of products were obtained when the catalyst was placed in the top part, in the 10th basket above superimposed nine empty identical baskets. The empty bottom basket rested on a thin steel bar welded across the tube, positioned 170 mm from the lower end of the main reactor body. This was also the location of the K-type thermocouple monitoring the reactor temperature to ensure the desired furnace

Table 3 – Parameters for lab-scale reactor model of acetic acid steam reforming.

Description	Value
Inlet pressure (bar)	1.05
Catalyst particle size (m)	2×10^{-4}
Apparent catalyst density $\rho_{cat,app}$ (kg m^{-3})	1640
Bed voidage ϵ_b (–)	0.4
Bed length L (m)	1.6×10^{-2}
Bed diameter (m)	9×10^{-3}

control temperature of the HZ was reached inside the reactor in each experiment. In the closed furnace, the bottom of the catalyst plug was therefore roughly 1/3 down in the HZ (or 2/3 up in the HZ), vertically 92 mm away from the furnace control thermocouple and 172 mm away from the inner reactor thermocouple, as shown in Fig. 1. Given how well the catalyst was embedded in the uniform temperature HZ, there was confidence that the control temperature represented the catalyst temperature accurately, itself not directly accessible.

To protect the gas analysers, moisture was removed from the gas in two stages. The bulk of the moisture was removed in a condenser, consisting of a jacketed heat exchanger cooled by a 1:1 mix of water and ethylene glycol at 4 $^{\circ}\text{C}$, followed by a series of three knock-out pots. Remaining traces of water were removed by a moisture trap filled with silica gel. The dry gas was passed through an ABB Advanced Optima analyser fitted with a Uras 14 module to measure CO, CO₂ and CH₄ by infrared absorption, and a Caldos 15 module for H₂ measurement by thermal conductivity detection (with correction accounting for CO, CO₂ and CH₄ content). Fluctuations in these measurements were minimised by using feed tubing with the smallest diameter available (1/16 in. OD). The experimental set-up was used to find AcOH conversion to C1 products, and outlet compositions at steady state. Reaction conditions were altered by changing the reactor temperature, S/C ratio and flow rates of N₂ and liquid. Table 2 summarises the experimental conditions that were used.

The conversions of reactants (AcOH and H₂O) were calculated via a series of mass balances. As the carrier gas (N₂) was inert, it could be assumed that the flow of N₂ remained the same at the inlet and outlet.

The number of moles of each component was calculated using Eq. (2) on the basis on N₂ concentration via the nitrogen balance in Eq. (1):

$$n_{dry,out} = \frac{n_{N_2,in}}{y_{N_2,out}} \quad \text{Eq. 1}$$

$$\text{and } n_{i,out} = y_{i,out} \times n_{dry,out} \quad \text{Eq. 2}$$

where $n_{dry,out}$ is the total molar flow of dry product gas, $n_{i,out}$ is the dry molar flow of product species i (e.g. $i = N_2, H_2, CH_4, CO, CO_2$ in Eqs (2)–(4)), and y_i is the molar fraction of i in the dry relevant product gas, additional subscripts ‘in’ (used for $N_2, AcOH$ and H_2O in Eqs (1), (3) and (4)) and ‘out’ (used for all species in Eqs (1)–(6)), refer to feed and outlet flows respectively.

The outlet flow of $AcOH$ was calculated by a carbon balance (Eq. (3)), while the outlet flow of H_2O was calculated by a hydrogen balance (Eq. (4)):

$$n_{AcOH,out} = n_{AcOH,in} - n_{dry,out} \times \left(\frac{y_{CO,out} + y_{CO_2,out} + y_{CH_4,out}}{2} \right) \quad \text{Eq. 3}$$

$$n_{H_2O,out} = \frac{4n_{AcOH,in} - 4n_{AcOH,out} + 2n_{H_2O,in} - n_{dry,out} (2y_{H_2} + 4y_{CH_4})}{2} \quad \text{Eq. 4}$$

The conversions of $AcOH$ to C1 products and water were then calculated as follows:

$$X_{AcOH} = \frac{n_{AcOH,in} - n_{AcOH,out}}{n_{AcOH,in}} \times 100\% \quad \text{Eq. 5}$$

$$X_{H_2O} = \frac{n_{H_2O,in} - n_{H_2O,out}}{n_{H_2O,in}} \times 100\% \quad \text{Eq. 6}$$

To examine carbon deposition and close the carbon balance, CHN analysis of the used catalyst (wt% carbon) was carried out, and the results used to estimate the conversion of the acetic acid to solid carbon. Around 15 mg of catalyst was placed into a tin capsule. The capsule was compressed to eliminate air before being placed onto an auto-sampler for analysis in a Flash EA 2000 elemental analyser where oxygen (BOC, purity 99.99%) was used as the oxidant, while helium (BOC, purity 99.99%) was used as carrier gas. The readings from CHN were converted to a molar amount using the following equation:

$$n_{C,solid} = m_{catalyst} X_C M_C \quad \text{Eq. 7}$$

where $n_{C,solid}$ is the number of moles of solid carbon produced during time t , and $m_{catalyst}$ is the mass of catalyst. x_C is the measured mass fraction of carbon, and M_C is the molar mass of carbon. The fractional conversion from $AcOH$ to solid carbon (X_{solid}) was found by:

$$X_{solid} = \frac{n_{C,solid}}{n_{C,AcOH,in} t} \quad \text{Eq. 8}$$

where $n_{C,AcOH,in}$ is the molar flow rate of carbon in acetic acid (2 mol of carbon for each mole of acetic acid) and t is the total experiment time.

Each experiment initially underwent a transient period before reaching steady state and was run twice; each run was included in the model fitting process. To obtain data for the kinetic study, $AcOH$ and H_2O conversions were taken only from the steady state period, typically starting around 10 min after the start of each run. There are different reasons for the 10 min transient period from the start of the reactants feed.

One is the time taken for feeds to travel through the system and reach the analysers, another is initial coke deposition (<1% of feed carbon) concentrated in the initial part of the runs, as discussed in the results section (carbon deposition).

Kinetic model

Modelling of lab-scale reactor

Kinetic parameters were found via the parameter estimation facility in gPROMS® [49,50], the process of which is summarised in the [Supplementary Data file](#). The parameter fitting operation required a model to describe the laboratory reactor, modelled as a packed bed reactor in steady state. The model used the mass balance equation in Equation (9), and as the reactor was considered isothermal, the energy equation was not solved.

$$\frac{\partial u C_i}{\partial z} = (1 - \epsilon_b) \rho_{cat,app} r_i \quad \text{Eq. 9}$$

where u is the superficial velocity ($m s^{-1}$), C_i is the gas phase concentration of species i ($mol m^{-3}$), z is the axial direction ($z = 0$ at inlet, $z = L$ at reactor exit), ϵ_b is the bed voidage, $\rho_{cat,app}$ is the apparent catalyst density ($kg m^{-3}$), and r_i is the rate of reaction consuming i ($mol kg^{-1} s^{-1}$).

We show in the results section, with further details in [Supplementary Data](#), that external mass transfer was not limiting, and the axial dispersion term was eliminated. Similarly, as the internal mass transfer was not limiting, the effectiveness factor was set to 1. All other assumptions and governing equations are as outlined in [Supplementary Data](#).

The physical properties of the reactor system are summarised in [Table 3](#). The inlet pressure was assumed to be slightly above atmospheric pressure, to account for the pressure drop through the system. Apparent density of the catalyst was calculated from the bed size and mass of catalyst, assuming a bed voidage of 0.4.

A gPROMS® parameter estimation problem requires the user to define control variables and measured data. In this case, the control variables were those experimental parameters that were altered, namely the inlet concentration, molar flux, and temperature. The measured data were the outlet conversions of acetic acid and H_2O , as described earlier.

The average relative error (ARE) was used to assess the accuracy of the model for the different output parameters. This was defined as follows:

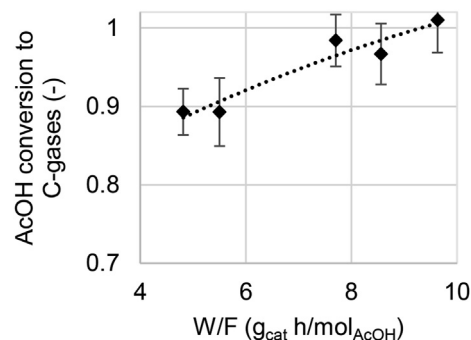


Fig. 2 – Experimental results used for calculation of mass transfer limitations (650 °C, with S/C = 3, $y_{N_2} = 0.6$).

Table 4 – Determination of internal and external mass transfer limitations.

Parameter	Value	
Measured rate of reaction (mol kg _{cat} ⁻¹ h ⁻¹)	31.24	
Particle radius (μm)	100	
Catalyst bulk density (kg m ⁻³) [51]	1200	
C _{bio,g} (mol m ⁻³)	0.768	
Diffusion volume v _{bio} [52]	51.88	
D _{bio,N₂} in cm ² s ⁻¹	0.878	
External mass transfer	Reynolds number (–)	0.465
	Schmidt number (–)	1.28
	Sherwood number (–)	2.44
	Mass transfer coefficient k _c (m s ⁻¹)	1.07
	Reaction order, assumed	1
	Mears criterion (–)	1.26 × 10 ⁻³
Internal mass transfer	Constriction factor σ _c [51]	0.8
	Tortuosity τ [51]	3.54
	Particle porosity [51]	0.59
	Effective diffusivity D _e (cm ² s ⁻¹)	0.117
	Weisz-Prater criterion (–)	1.16 × 10 ⁻²
	Effectiveness factor (–)	0.999

$$ARE = \frac{1}{N} \sum_{j=1}^N \frac{|y_{predicted,j} - y_{measured,j}|}{y_{measured,j}} \times 100\% \quad \text{Eq. 10}$$

where $y_{predicted,j}$ and $y_{measured,j}$ represent the measured and predicted values of a parameter at point j , such as reactant conversion or species concentration.

Results and discussion

Mass transfer limitations were assessed using a set of experiments at the highest experimental temperature (650 °C), where mass transfer was most likely to be limiting. The results of the experiments are shown on Fig. 2.

The curve was fit to a second order polynomial, with $R^2 = 0.9191$:

$$X_{AcOH} = -0.0012 \left(W/F \right)^2 + 0.0428 \left(W/F \right) + 0.7082 \quad \text{Eq. 11}$$

Where W/F is the pseudo contact time.

The polynomial was differentiated to give an equation for rate of reaction:

$$\frac{dX_{AcOH}}{dW/F} = -r_{AcOH} = -0.0024 \left(W/F \right) + 0.0428 \quad \text{Eq. 12}$$

The estimated rate of reaction was used to find the Mears criterion, Weisz-Prater criterion and effectiveness factor. Results are summarised in Table 4, showing that neither external nor internal mass transfer were limiting at the conditions used in this study.

Experimental measurements of reactant conversion

The following figures summarise the experimental data that was collected, showing how conversions varied as temperature and S/C ratio were changed. The data follows the

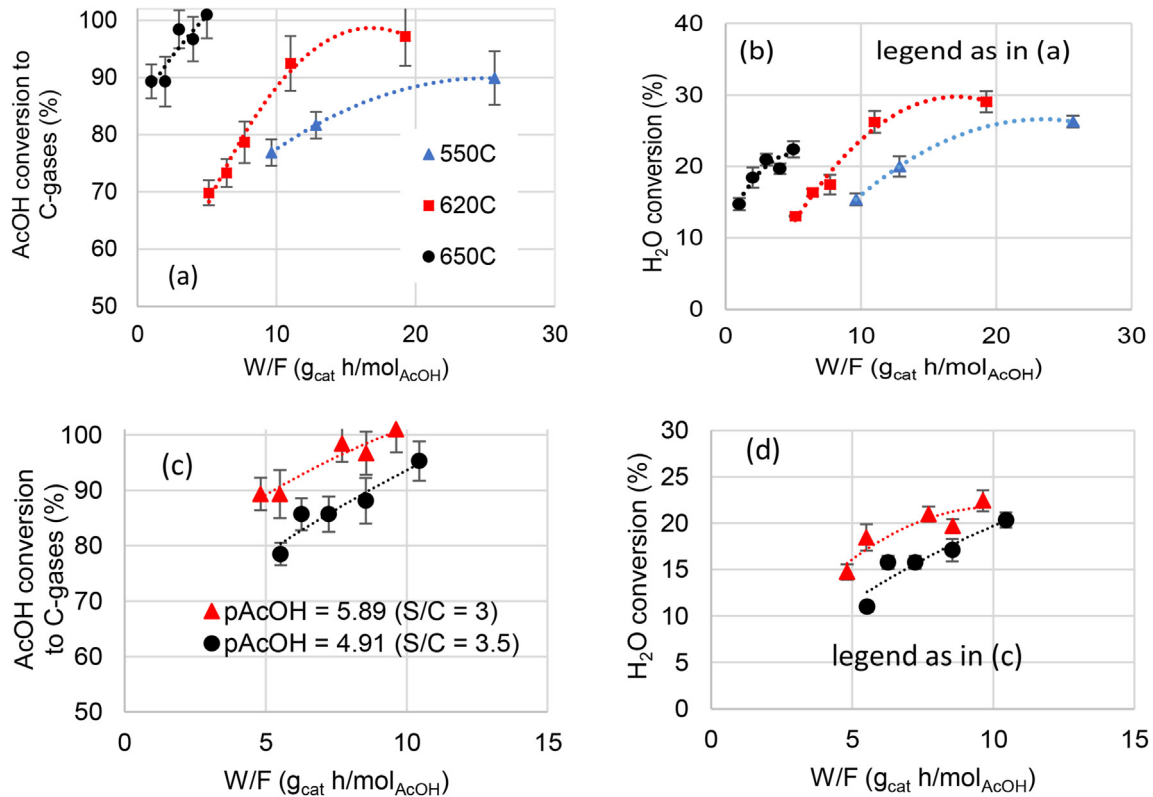


Fig. 3 – Conversion vs pseudo contact time for different temperatures at S/C = 3, p_{AcOH} = 5.89, p_{H₂O,0} = 34.64 kPa. (a) AcOH and (b) H₂O, and for different partial pressures of AcOH at 650 °C, p_{H₂O,0} = 34.64 kPa. (c) AcOH and (d) H₂O.

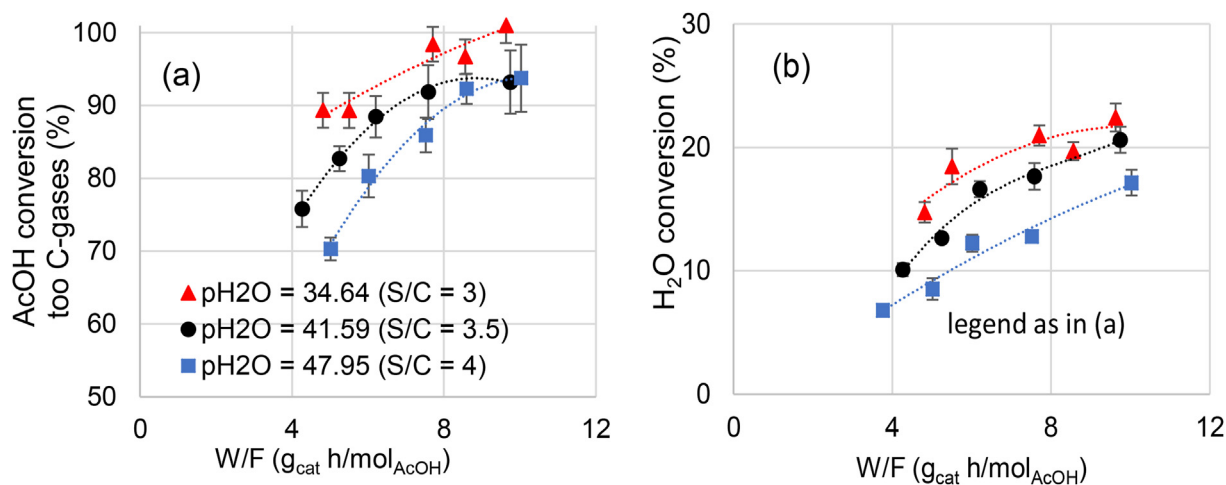


Fig. 4 – Conversion vs pseudo contact time ($W/F_{AcOH,0}$) for different partial pressures of H_2O at $650\text{ }^\circ\text{C}$, $p_{AcOH,0} = 5.89\text{ kPa}$. (a) AcOH and (b) H_2O .

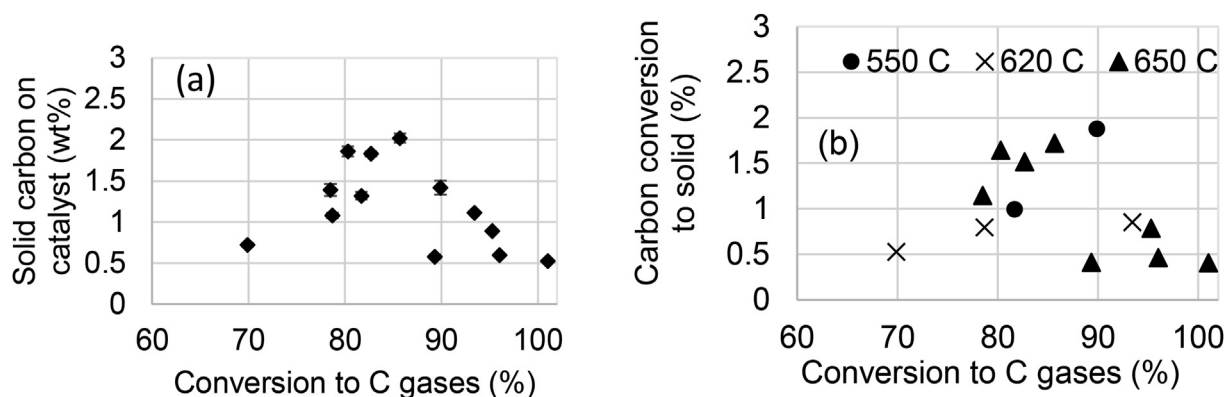


Fig. 5 – (a) Carbon content in used catalyst vs conversion to C-gases, error bars show standard deviations of duplicate samples and (b) Conversion to solid carbon vs conversion to C-gases for same runs as (a), shown by run temperature.

expected trends, with conversion increasing with pseudo-contact time. Other observed trends are an increase of conversion with temperature or with partial of pressure of AcOH (Fig. 3). Fig. 4 shows a decrease in AcOH conversion as S/C ratio increased. As steam was in excess ($S/C > 1$), increasing the S/C ratio did not improve AcOH conversion. Instead, the trend may be explained by the change in flow rates. Increasing S/C ratio decreases the pseudo-contact time for water ($W/F_{H_2O,0}$) and thus reduces its opportunity to react with AcOH.

Carbon deposition

Samples of used catalyst were subjected to CHNS analysis, to examine the extent of carbon deposition. The carbon content in the catalyst and therefore the conversion of the carbon feed to solid carbon changed with the conversion to carbon gases, as shown in Fig. 5.

The results confirm that the level of carbon deposition was low (on average 1% of the feed), due to operation at high

Table 5 – Reaction schemes in proposed kinetic models.

Reaction (R _i from Table 1)	Stoichiometry	Model		
		1	2	
R1	Steam reforming acetic acid	$CH_3COOH + 2H_2O \rightarrow 2CO_2 + 4H_2$	✓	✓
R2	Decomposition 1	$CH_3COOH \rightarrow 2CO + 2H_2$	✓	✓
R3	Decomposition 2	$CH_3COOH \rightarrow CH_4 + CO_2$		✓
R4	SMR	$CH_4 + H_2O \leftrightarrow CO + 3H_2$		✓
R5	Water gas shift 'WGS'	$CO + H_2O \leftrightarrow H_2 + CO_2$	✓	✓

Table 6 – Rate equations for Models 1A and 1B, reactions listed in Table 5.

Reaction	Rate equation
R1	$R_1 = k_1 p_{\text{AcOH}}^{\alpha_1}$
R2	$R_2 = k_2 p_{\text{AcOH}}^{\alpha_2}$
R5	Model 1A:
	Model 1A: $R_{5a} = \frac{k_{5a}}{p_{\text{H}_2}} \left(p_{\text{CO}} p_{\text{H}_2\text{O}} - \frac{p_{\text{H}_2} p_{\text{CO}_2}}{K_{\text{WGS}}} \right) \left(\frac{1}{\Omega^2} \right)$
	$\Omega = 1 + K_{\text{CO}} p_{\text{CO}} + K_{\text{H}_2} p_{\text{H}_2} + K_{\text{CH}_4} p_{\text{CH}_4} + K_{\text{H}_2\text{O}} \frac{p_{\text{H}_2\text{O}}}{p_{\text{H}_2}}$
	$K_{\text{WGS}} = \exp\left(\frac{4400}{T} - 4.036\right)$
	Model 1B:
	$R_{5b} = k_{5b} \left(p_{\text{CO}} p_{\text{H}_2\text{O}} - \frac{p_{\text{H}_2} p_{\text{CO}_2}}{K_{\text{WGS}}} \right)$
	$K_{\text{WGS}} = \exp\left(a + \frac{b}{T} + c \log(T) + dT + eT^2 + \frac{f}{T^2}\right)$
	$a = -18, b = 5.8 \times 10^3, c = 1.8,$
	$d = -2.7 \times 10^{-4}, e = 0, f = -5.8 \times 10^4$

Table 7 – Rate equations for Models 2A and 2B, reactions listed in Table 5.

Reaction	Rate equation
R1, R2, R5	Rate equation and nomenclature as in Table 6
R3	$R_3 = k_3 p_{\text{AcOH}}^{\alpha_3}$
R4	$R_4 = k_4 \left(p_{\text{CH}_4} p_{\text{H}_2\text{O}} - \frac{p_{\text{H}_2}^3 p_{\text{CO}}}{K_{\text{SMR}}} \right)$
	$K_{\text{SMR}} = \exp\left(a + \frac{b}{T} + c \log(T) + dT + eT^2 + \frac{f}{T^2}\right)$
	$a = -24.9, b = -2.278 \times 10^4, c = 7.951,$
	$d = -4.354 \times 10^{-3}, e = 3.607 \times 10^{-7}, f = 4850$

temperature with an excess of steam. Fig. 5b shows the carbon conversion to solid C in % of the feed, vs. the conversion to gases for the three temperatures, but a clear trend of temperature on solid C cannot be seen. Morphology of the carbon

deposited during runs at 650 °C and S/C of 3 is shown in TEM images in [14] with evidence of amorphous carbon. In addition, each experiment shown in Fig. 5 was run for only a short time (around 10–20 min), so there was limited time for deactivation to occur. For this study it was assumed that carbon deposition had a minimal impact on catalyst activity. Future work might also consider the rate of catalyst deactivation in its experimental design. For example, the kinetic studies on bio-oil by Arregi et al. [53], Barbarias et al. [54] and Gayubo et al. [55] included a term for catalyst activity in each rate equation:

$$r_i = r_j a \quad \text{Eq. 13}$$

where r_i is the rate of reaction including catalyst deactivation, and r_j is the rate of reaction before deactivation. The term a signifies the catalyst activity.

By running the experiments for long durations (>100 min), the authors of these studies were able to derive the rate of catalyst deactivation, i.e. the rate of change of a . A similar method could be applied in a future study in order to improve the model.

Parameter fitting

On the basis of the literature review, two simplified reaction schemes were evaluated, termed Model 1 and Model 2. These considered only the major reactions, in order to minimise the number of parameters to be fitted. Model 1 contained three reactions: steam reforming of AcOH (R1), decomposition of AcOH to syngas (R2), and water gas shift (R5). In addition to the reactions of Model 1, Model 2 also included decomposition to methane, and steam methane reforming (SMR), in order to examine whether a more detailed mechanism could improve accuracy. Models 1 and 2 were chosen over models using acetone as an intermediate, based on equilibrium products prediction, and in agreement with the findings on nickel catalysts of Phongruksathat et al. [48]. Model 1 did not include

Table 8 – Kinetic parameters estimated by gPROMS parameter fitting.

Reaction parameters		Model			Literature
		1A	1B	2B	
k_{01}	($\text{mol kg}_{\text{cat}}^{-1} \text{bar}^{-\alpha_1} \text{s}^{-1}$)	0.778	0.867	0.0765	–
E_{A1}	(kJ mol^{-1})	60.85	60.40	122.73	–
α_1	(–)	0.958	0.953	1.20	–
k_{02}	($\text{mol kg}_{\text{cat}}^{-1} \text{bar}^{-\alpha_2} \text{s}^{-1}$)	0.955	0.648	0.0662	–
E_{A2}	(kJ mol^{-1})	61.25	51.70	40.70	–
α_2	(–)	0.636	0.823	0.578	–
k_{03}	($\text{mol kg}_{\text{cat}}^{-1} \text{bar}^{-\alpha_3} \text{s}^{-1}$)	–	–	7.994	–
E_{A3}	(kJ mol^{-1})	–	–	83.01	–
α_3	(–)	–	–	1.123	–
k_{04}	($\text{mol kg}_{\text{cat}}^{-1} \text{bar}^{-2} \text{s}^{-1}$)	–	–	8.6×10^3	0.542 [55]
E_{A4}	(kJ mol^{-1})	–	–	194.82	357.50 [55]
$k_{05,a}$	($\text{mol kg}_{\text{cat}}^{-1} \text{bar}^{-1} \text{s}^{-1}$)	4299	–	–	5.43×10^5 to 9.9×10^6 [56,57]
$k_{05,b}$	($\text{mol kg}_{\text{cat}}^{-1} \text{bar}^{-2} \text{s}^{-1}$)	–	607	68.54	5.0 to 360 [53–55]
E_{A5}	(kJ mol^{-1})	94.65	86.71	67.13^a	30.00 to 89.23 [53–57]
ARE	X_{AcOH} (%)	5.37	4.43	6.01	–
	$X_{\text{H}_2\text{O}}$ (%)	6.36	10.46	8.94	–
	$Y_{\text{CH}_4, \text{dry}}$ (%)	–	–	27.5	–
R2		98.8	99.0	99.3	–

^a Activation energy fixed at the value from Xu and Froment [56], to enable convergence. Further information in text.

reactions relating to methane, as the experiments yielded very low CH_4 contents (<1 vol%), also in agreement with [48]. The reaction steps in the proposed kinetic models are shown in Table 5 making use of reactions listed in Table 1.

Table 6 and Table 7 summarise the reaction schemes used in each of the proposed models. Primary reactions involving acetic acid (R1-R3) were modelled via simple power law rate equations, an approach typically used for irreversible global reactions. The concentration of water was not included in the power law rate equation for R1, as water was in large excess ($S/C = 3-4$), compared to the stoichiometric S/C of 1. SMR and WGS reactions were described using equilibrium rate equations reactions from literature [53,55].

Two different versions of the WGS rate equation were used. Version A, used in Models 1A and 2A, was a more complex form, taken from Xu and Froment [56]. However,

initial testing found that Model 2A was not able to converge with this form of the equation. Thus a simplified version of the WGS rate equation (versions 'B') was also trialled, based on previous bio-oil kinetic studies [53,54]. The simplified WGS rate equation was used in Models 1B and 2B.

These rate equations were entered into the gPROMs model, and the measured experimental data was used to perform parameter fitting. The results of the parameter fitting are given in Table 8. No values are given for Model 2A, as the parameter fitting was unable to converge due to the more complex WGS reaction rate.

Model 2B was initially unable to converge, due to the large number of unknown parameters. To enable convergence, the activation energy of the WGS reaction (E_{AS}) was fixed, using a value from literature. A value of 67130 J mol^{-1} was taken from Xu and Froment [56]. A sensitivity analysis showed that

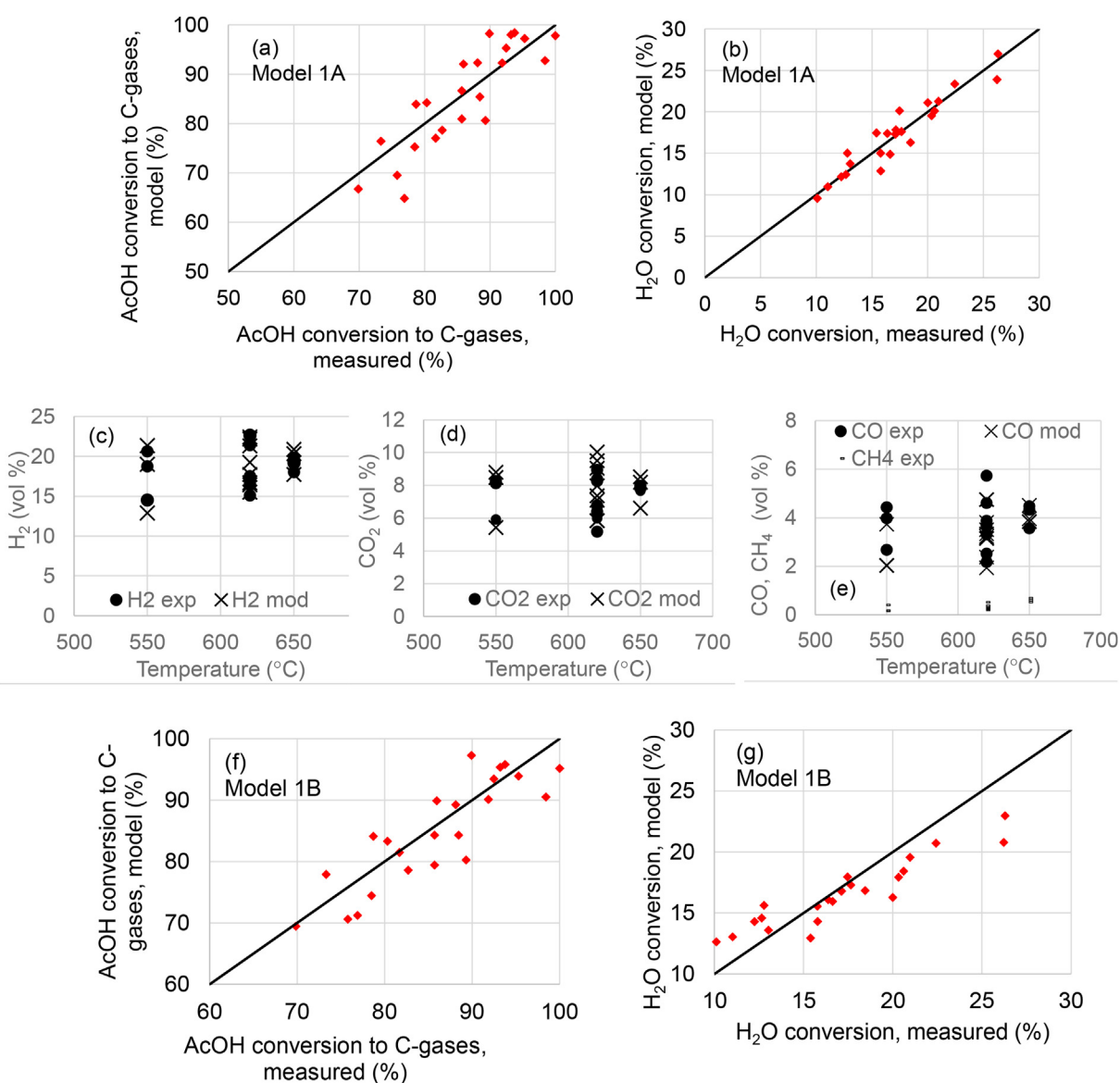


Fig. 6 – Comparisons experiments vs. Model 1A (a–b) parity plots of AcOH and H₂O conversion for full range of S/C, Temperature and W/F studied, (c–e) vol% of H₂, CO₂, CO and CH₄ vs. temperature at S/C 3 for all the W/F values, and vs. Model 1B (f–g) parity plots of AcOH and H₂O conversion, full range of experiments.

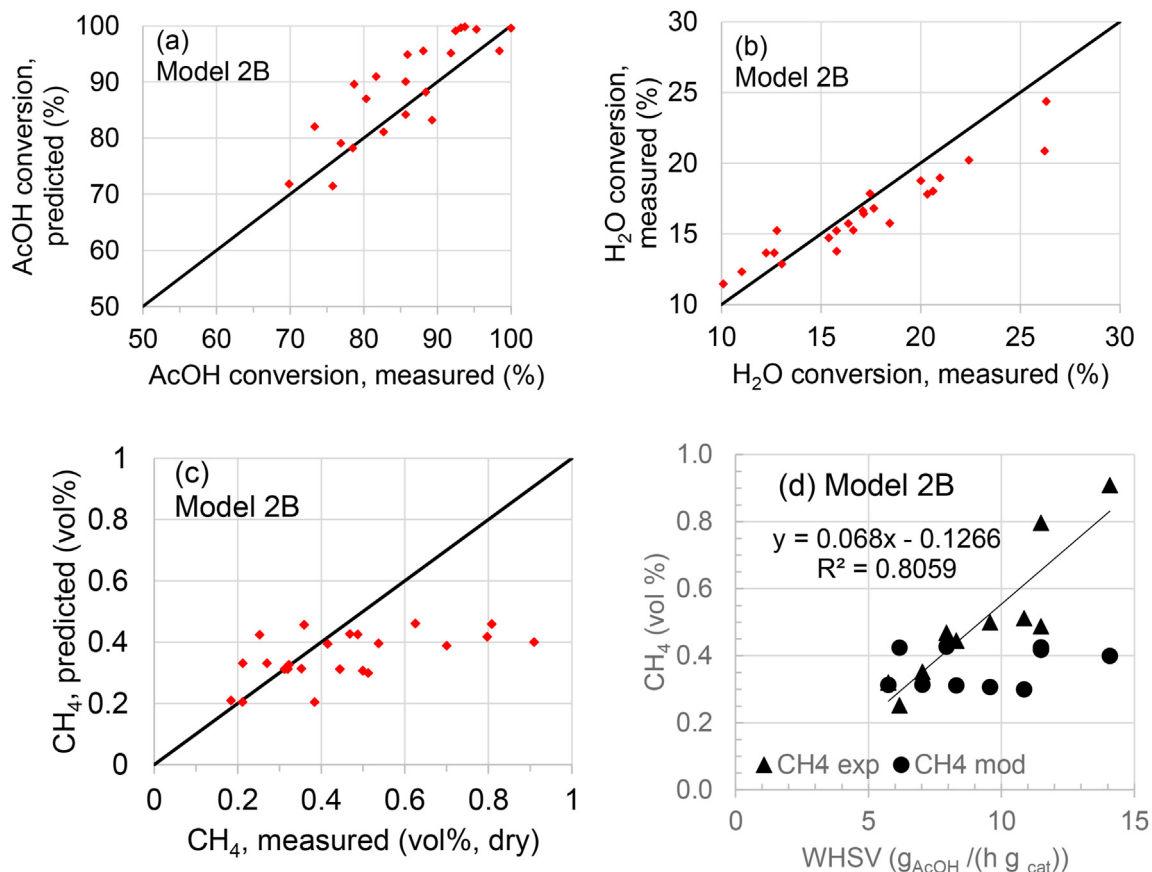


Fig. 7 – Comparison experiments - Model 2B (a–c) parity plots for AcOH conversion, H₂O conversion and CH₄ in outlet gas for full range of temperature, S/C and W/F studied, (d) CH₄ vol % vs. WHSV (=1/(W/F) for S/C 3 and 650 °C, with linear fit on exp.

changing this value of E_{A5} by $\pm 50\%$ had a minimal impact on overall accuracy (ARE + 2%). Future studies on this catalyst may focus exclusively on the WGS reaction, in order to confirm the most accurate value to use. However, for the purposes of this study, the value from Xu and Froment [56] was deemed suitable.

The goodness of fit for each of the models is shown in Fig. 6 (models 1A and 1B) and Fig. 7 (model 2B). In Fig. 6 (a–e), Model 1A appears to give a good fit for conversion of both reactants as well as products, with results on reactants conversion close to the parity line and without any skew, and near superimposed experimental and modelling products vol %.

Fig. 6f shows that Model 1B gives a good fit for AcOH conversion, but there is a skew on the H₂O conversion results in Fig. 6g. This may be associated with the less detailed form of the WGS equation. Model 2B, which used the same form of the WGS equations, had a similar skew (Fig. 7b).

Model 2B appears to give a reasonably good fit for AcOH conversion (Fig. 7a), and some skew for H₂O conversion (Fig. 7b), similar to Model 1B. However, the poor fit shown in the parity plot for CH₄ in Fig. 7c suggests that the model is not providing an accurate description of the underlying mechanisms involving methane.

Fig. 7d shows that the methane concentration in the products for S/C 3 and 650 °C runs, all below 1 vol%, increased with increasing weight hourly space velocity (WHSV = 1/(W/

F)), but that this trend is not matched by the model. It is worth noting that trying to fit methane concentrations when the experimental values are so near the lower limit of the analyser's detection may not be worthwhile.

Table 8 gives a quantitative basis for comparison. Model 1A provides the best fit for H₂O conversion (average relative error 'ARE' of 5.37%). Model 1B gives a slightly better accuracy for AcOH conversion (ARE of 4.43%), but the accuracy of H₂O conversion is reduced considerably, to give an ARE over 10%. Thus Model 1A gives the best fit when both reactants are considered together. On the basis of these results, Model 1A was judged to give the best fit and was carried forward for further study in the following sections.

Statistics on the goodness of the fits for models 1A, 1B and 2B are provided in the supplementary data file.

Kinetic model validation

After Model 1A provided a satisfactory fit for reactant conversions, the model was further tested by comparing predicted outlet compositions to experimental and equilibrium results.

Model testing away from equilibrium

To test the model at conditions away from equilibrium, the outlet compositions predicted by the reactor model were

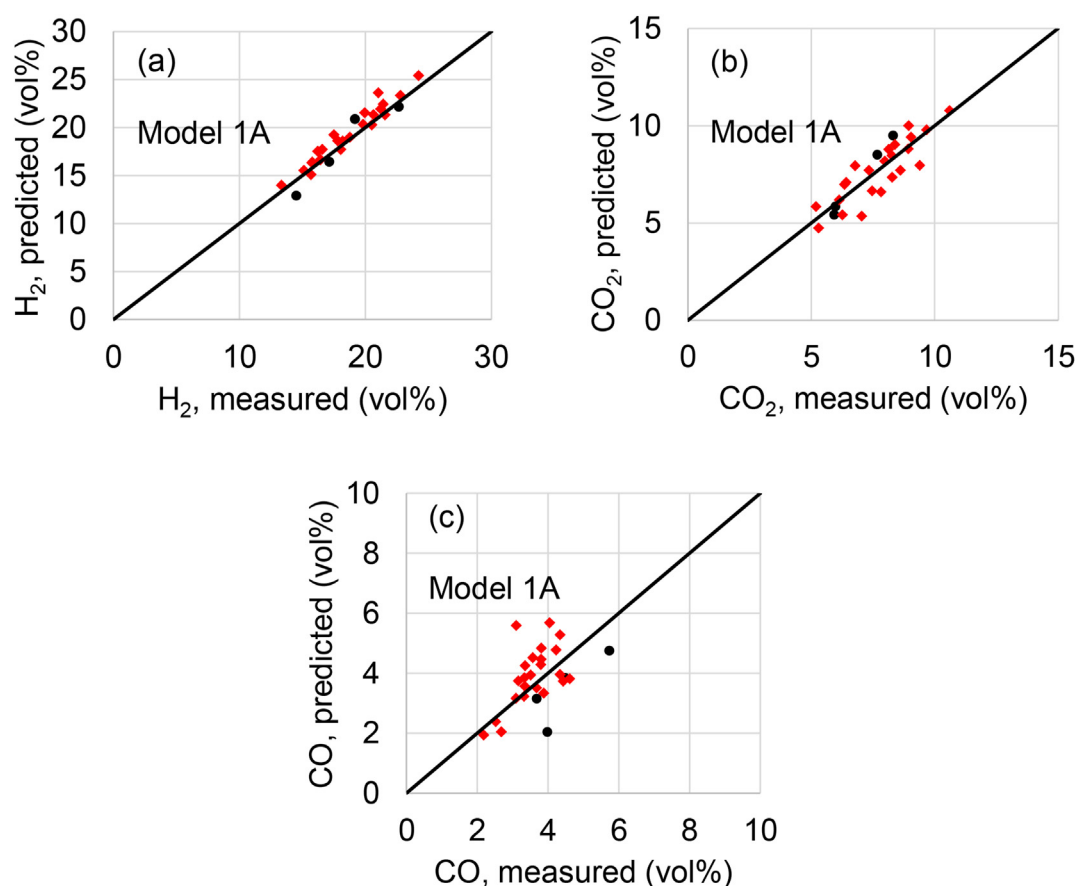


Fig. 8 – Parity plots for outlet compositions from Model 1A (a) H₂ vol%, (b) CO₂ vol% and (c) CO vol%. Red dots signify experiments used in parameter fitting, black dots signify experiments not used in the original parameter fitting. (For interpretation of the references to colour in this figure legend, the reader is referred to the Web version of this article.)

compared to those measured during experiments. To provide extra validation, four extra experiments were included that were not within the original parameter fitting. The parity plots for outlet composition are given below. Fig. 8a and Fig. 8b demonstrate a good fit for H₂ and CO₂ content, even for those experiments that were not included in the parameter fitting (signified as black dots). Fig. 8c shows the fitting for CO is also reasonably good, although not as accurate as the other components.

Table 9 shows the accuracy of predicted outlet concentrations. The model shows good accuracy for H₂ concentration, with an ARE around 4%. There is greater error for the compounds that contain carbon, particularly CO. This suggests that there is opportunity to improve the model by refining reactions involving CO, such as decomposition and WGS. Nonetheless, the average of the three components's AREs is less than 11%, suggesting the model is suitable for preliminary estimates relating to reactor size and H₂ yield.

Model testing at equilibrium

To further test the model, gPROMS model outputs at equilibrium were compared against those from an Aspen Plus® equilibrium reactor ('RGibbs') at the same conditions. The Peng-Robinson property method [58] was used as recommended for H₂ rich, high temperature and high pressure mixtures such as in reforming of bio-oil and acetic acid and

used in previous relevant Aspen Plus simulations [33,59,60]. The effects of temperature, S/C ratio and pressure were examined. Fig. 9a-b shows that the kinetic model provides a good estimation in the temperature region 600–700 °C, but outside of this region the model results diverge from equilibrium results. Fig. 9c-d shows that the model is not readily extrapolated to pressures outside the experimental range, as it relies on an empirical power law equation.

For both temperature and pressure, the area of highest accuracy is the region where there is little methane formation, i.e. at high temperature and/or low pressure. This is to be expected, as the simplified kinetic model does not consider methane formation. It highlights that caution is to be advised when extrapolating this kinetic model to low temperature and/or high pressure regions where CH₄ formation is likely.

Fig. 10 shows the kinetic model provides a good match to equilibrium results at a range of S/C ratios. As the experiments

Table 9 – Accuracy of predicted vs measured outlet concentrations (Model 1A).

Component	ARE (%)
$y_{H_2, dry}$	4.34
$y_{CO, dry}$	18.46
$y_{CO_2, dry}$	9.12
Average of ARE (%)	10.64

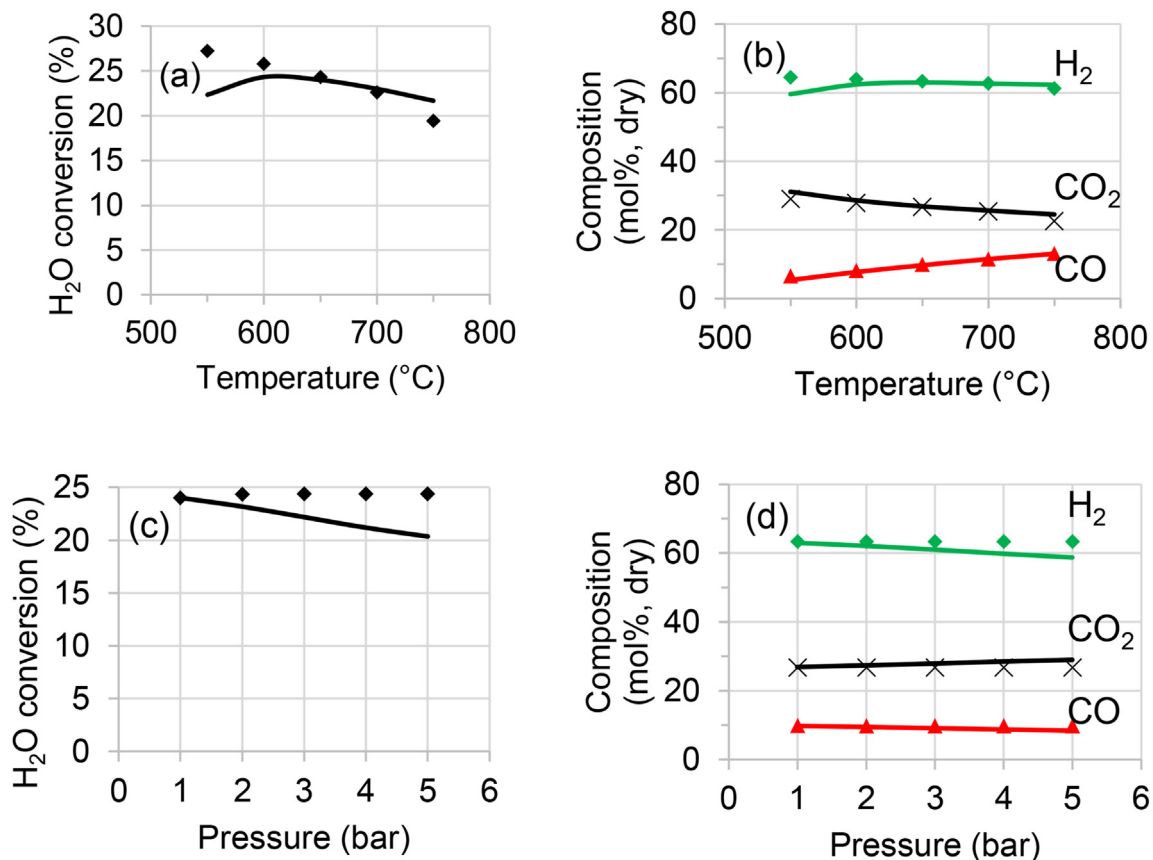


Fig. 9 – Effect of temperature on (a) H₂O conversion, (b) H₂, CO and CO₂ content at equilibrium. Inlet conditions are 1 bar, S/C = 3. Effect of pressure on (c) H₂O conversion, (d) H₂, CO and CO₂ content at equilibrium. Inlet conditions S/C = 3, 650 °C. Points represent kinetic model results, while solid lines represent Aspen Plus equilibrium results.

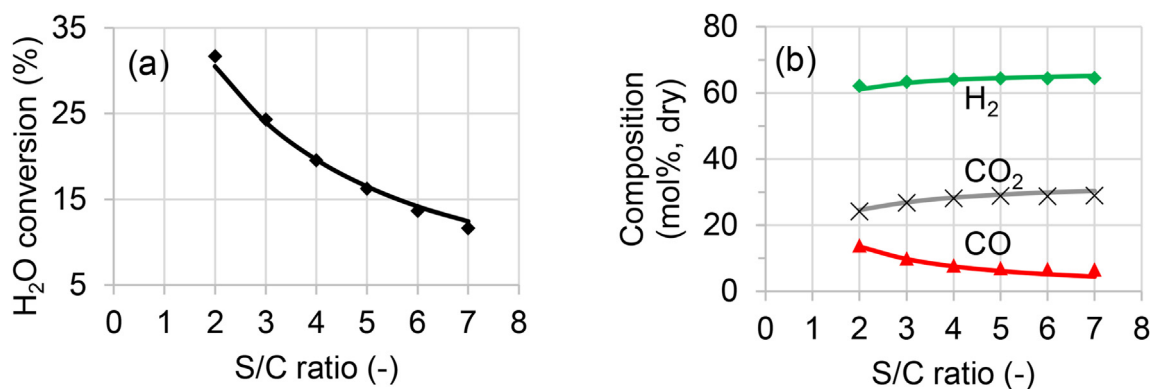


Fig. 10 – Effect of S/C ratio on (a) H₂O conversion, (b) H₂, CO and CO₂ content at equilibrium. Inlet conditions are 1 bar, 650 °C. Points represent kinetic model results, while solid lines represent Aspen Plus equilibrium results.

used an excess of steam, the model remains valid when this excess is increased further.

Conclusion

A kinetic study has been conducted for acetic acid steam reforming on an industrially produced nickel on calcium aluminate catalyst. After confirming the absence of mass transfer limitations, experimental data were used for

parameter fitting in gPROMS. Four kinetic models were proposed, which described simplified reaction schemes. Power law rate equations were used for the primary reactions of acetic acid. Secondary reactions SMR and WGS were described by mass action rate equations from literature. Of the models tested, the model consisting of steam reforming of AcOH to CO₂ and H₂, AcOH decomposition to syngas, and water gas shift, was found to be the most accurate, with H₂ concentration in average within a 4% relative error of the measured value. Testing against equilibrium results showed that this

model provided a good fit for near atmospheric pressure conditions in the temperature region 600–700 °C, with S/C ratios ranging from 3 to 8. Such a model could be a subset of future models of Ni-catalysed steam reforming of more complex mixtures representative of bio-oils or organic waste streams for process design and optimisation purposes, for conditions of excess of steam and temperatures above 550 °C, and where the water gas shift reaction would feature as an essential common step.

Declaration of competing interest

The authors declare that they have no known competing financial interests or personal relationships that could have appeared to influence the work reported in this paper.

Acknowledgments

This research was funded by EPSRC Bioenergy Centre for Doctoral Training, grant number EP/L014912/1 (PhD studentship to J. Reeve), and UKCCSRC EPSRC consortium Call 2 grant “Novel Materials and Reforming Process Route for the Production of Ready-Separated CO₂/N₂/H₂ from Natural Gas Feedstocks”, grant number EP/K000446/1 for license costs of Aspen Plus.

Associated data can be found at <https://doi.org/10.5518/1208>.

Appendix A. Supplementary data

Supplementary data to this article can be found online at <https://doi.org/10.1016/j.ijhydene.2022.08.167>.

REFERENCES

- [1] Pimenidou P, Dupont V. Characterisation of palm empty fruit bunch (PEFB) and pinewood bio-oils and kinetics of their thermal degradation. *Bioresour Technol* 2012;109:198–205.
- [2] Zin RM, Lea-Langton A, Dupont V, Twigg MV. High hydrogen yield and purity from palm empty fruit bunch and pine pyrolysis oils. *Int J Hydrogen Energy* 2012;37:10627–38.
- [3] Ringer M, Putsche V, Scahill J. Large-scale pyrolysis oil production: a technology november 2006 assessment and economic analysis. Prepared under task No. BB06.7510. Technical report. 2006.
- [4] Sukiran MA, Chin CM, Bakar NKA. Bio-oils from pyrolysis of oil palm empty fruit bunches. *Am J Appl Sci* 2009;6(5):869–75. 2009; 6:869-875.
- [5] Bridgwater AV, Meier D, Radlein D. An overview of fast pyrolysis of biomass. *Org Geochem* 1999;30:1479–93.
- [6] Hoang TMC. Catalytic gasification of humin based by-product from biomass processing – a sustainable route for hydrogen. Twente: University of Twente; 2014.
- [7] González-Arias J, Sánchez ME, Cara-Jiménez J, Baena-Moreno FM, Zhang Z. Hydrothermal carbonization of biomass and waste: a review. *Environ Chem Lett* 2021;20:211–21.
- [8] Wu D, Li L, Zhao X, Peng Y, Yang P, Peng X. Anaerobic digestion: a review on process monitoring. *Renew Sustain Energy Rev* 2019;103:1–12.
- [9] Borges RP, Ferreira RAR, Rabelo-Neto RC, Noronha FB, Hori CE. Hydrogen production by steam reforming of acetic acid using hydrotalcite type precursors. *Int J Hydrogen Energy* 2018;43:7881–92.
- [10] Basagiannis AC, Vverykios XE. Catalytic steam reforming of acetic acid for hydrogen production. *Int J Hydrogen Energy* 2007;32:3343–55.
- [11] Wang Z, Sun L, Chen L, Yang S, Xie X, Gao M, et al. Steam reforming of acetic acid for hydrogen production over Ni/CaxFeyO catalysts. *Int J Hydrogen Energy* 2021;46:33132–42.
- [12] Megía PJ, Carrero A, Calles JA, Vizcaíno AJ. Hydrogen production from steam reforming of acetic acid as a model compound of the aqueous fraction of microalgae HTL using Co-M/SBA-15 (M: Cu, Ag, Ce, Cr) catalysts. *Catalysts* 2019;9.
- [13] Omoniyi OA, Dupont V. Optimised cycling stability of sorption enhanced chemical looping steam reforming of acetic acid in a packed bed reactor. *Appl Catal B Environ* 2019;242:397–409.
- [14] Omoniyi OA, Dupont V. Chemical looping steam reforming of acetic acid in a packed bed reactor. *Appl Catal B Environ* 2018;226:258–68.
- [15] Tande LN, Resendiz-Mora E, Dupont V, Twigg MV. Autothermal reforming of acetic acid to hydrogen and syngas on Ni and Rh catalysts. *Catalysts* 2021;11.
- [16] Yun HAH, Ramírez-Solís S, Dupont V. Bio-CH₄ from palm empty fruit bunch via pyrolysis-direct methanation: full plant model and experiments with bio-oil surrogate. *J Clean Prod* 2020:244.
- [17] Soloviev SO, Gubareni IV, Orlyk SM. Oxidative reforming of methane on structured nickel–alumina catalysts: a review. *Theor Exp Chem* 2018;54:293–315.
- [18] Saguru C, Ndlovu S, Moropeng D. A review of recent studies into hydrometallurgical methods for recovering PGMs from used catalytic converters. *Hydrometallurgy* 2018;182:44–56.
- [19] European Commission a. Critical raw materials resilience: charting a path towards greater security and sustainability. Brussels: COMMUNICATION FROM THE COMMISSION TO THE EUROPEAN PARLIAMENT, THE COUNCIL, THE EUROPEAN ECONOMIC AND SOCIAL COMMITTEE AND THE COMMITTEE OF THE REGIONS; 2020.
- [20] Bobba S, Carrara S, Huisman J, Mathieux F, Pavel C. Critical raw materials for strategic technologies and sectors in the EU A foresight study. Brussels: European Commission, Joint Research Centre; 2020.
- [21] Mosley J. Final list of critical minerals. 2022.
- [22] Luo S, Zeng L, Fan LS. Chemical looping technology: oxygen carrier characteristics. *Annu Rev Chem Biomol Eng* 2015;6:53–75.
- [23] Cheng F, Dupont V. Steam reforming of bio-compounds with auto-reduced nickel catalyst. *Catalysts* 2017;7.
- [24] Ridler D, Twigg MV. Steam reforming. In: Twigg MV, editor. *Catalyst handbook*. 2nd ed. Butler & Tanner. Frome, England: Wolfe Publishing Ltd; 1989.
- [25] Wang Q, Xie W, Jia X, Chen B, An S, Xie X, et al. Ca–Al layered double hydroxides-derived Ni-based catalysts for hydrogen production via auto-thermal reforming of acetic acid. *Int J Hydrogen Energy* 2019;44:20007–16.
- [26] Hou Z, Yokota O, Tanaka T, Yashima T. A novel KCaNi/apha-Al₂O₃ catalyst for CH₄ reforming with CO₂. *Catal Lett April* 2003;87(1–2):37–42. 2003;87.
- [27] Vazquez Thyssen V, Moreira Assaf E. Ni/CaO-SiO₂ catalysts for assessment in steam reforming reaction of acetol. *Fuel* 2019;254.
- [28] Song JH, Han SJ, Yoo J, Park S, Kim DH, Song IK. Hydrogen production by steam reforming of ethanol over Ni–X/Al 2 O 3

- ZrO₂ (X = Mg, Ca, Sr, and Ba) xerogel catalysts: Effect of alkaline earth metal addition. *J Mol Catal Chem* 2016;415:151–9.
- [29] Garbarino G, Pugliese F, Cavattoni T, Busca G, Costamagna P. A study on CO₂ methanation and steam methane reforming over commercial Ni/calcium aluminate catalysts. *Energies* 2020;13.
- [30] Vagia EC, Lemonidou AA. Hydrogen production via steam reforming of bio-oil components over calcium aluminate supported nickel and noble metal catalysts. *Appl Catal, A* 2008;351:111–21.
- [31] Medrano J, Oliva M, Ruiz J, Garcia L, Arauzo J. Catalytic steam reforming of acetic acid in a fluidized bed reactor with oxygen addition. *Int J Hydrogen Energy* 2008;33:4387–96.
- [32] Rioche C, Kulkarni S, Meunier FC, Breen JP, Burch R. Steam reforming of model compounds and fast pyrolysis bio-oil on supported noble metal catalysts. *Appl Catal B Environ* 2005;61:130–9.
- [33] Gil MV, Fermoso J, Pevida C, Chen D, Rubiera F. Production of fuel-cell grade H₂ by sorption enhanced steam reforming of acetic acid as a model compound of biomass-derived bio-oil. *Appl Catal B Environ* 2016;184:64–76.
- [34] Xie H, Yu Q, Wang K, Shi X, Li X. Thermodynamic analysis of hydrogen production from model compounds of bio-oil through steam reforming. *Environ Prog Sustain Energy* 2014;33:1008–16.
- [35] Lemonidou AA, Vagia EC, Lercher JA. Acetic acid reforming over Rh supported on La₂O₃/CeO₂–ZrO₂: catalytic performance and reaction pathway analysis. *ACS Catal* 2013;3:1919–28.
- [36] Trane R, Dahl S, Skjøth-Rasmussen MS, Jensen AD. Catalytic steam reforming of bio-oil. *Int J Hydrogen Energy* 2012;37:6447–72.
- [37] Vagia E, Lemonidou A. Thermodynamic analysis of hydrogen production via autothermal steam reforming of selected components of aqueous bio-oil fraction. *Int J Hydrogen Energy* 2008;33:2489–500.
- [38] Bimbela F, Oliva M, Ruiz J, García L, Arauzo J. Hydrogen production by catalytic steam reforming of acetic acid, a model compound of biomass pyrolysis liquids. *J Anal Appl Pyrol* 2007;79:112–20.
- [39] Galdamez JR, Garcia L, Bilbao R. Hydrogen production by steam reforming of bio-oil using Co-precipitated Ni-Al catalysts. Acetic acid as a model compound. *Energy Fuels* 2005;19:10.
- [40] Iwasa N, Yamane T, Takei M, Ozaki J-i, Arai M. Hydrogen production by steam reforming of acetic acid: comparison of conventional supported metal catalysts and metal-incorporated mesoporous smectite-like catalysts. *Int J Hydrogen Energy* 2010;35:110–7.
- [41] Resende KA, Ávila-Neto CN, Rabelo-Neto RC, Noronha FB, Hori CE. Thermodynamic analysis and reaction routes of steam reforming of bio-oil aqueous fraction. *Renew Energy* 2015;80:166–76.
- [42] Chen G, Tao J, Liu C, Yan B, Li W, Li X. Hydrogen production via acetic acid steam reforming: a critical review on catalysts. *Renew Sustain Energy Rev* 2017;79:1091–8.
- [43] Wang D, Montane D, Chornet E. Catalytic steam reforming of biomass-derived oxygenates: acetic acid and hydroxyacetaldehyde. *Appl Catal, A* 1996;143:245–70.
- [44] Takanabe K, Aika K, Inazu K, Baba T, Seshan K, Lefferts L. Steam reforming of acetic acid as a biomass derived oxygenate: bifunctional pathway for hydrogen formation over Pt/ZrO₂ catalysts. *J Catal* 2006;243:263–9.
- [45] Wang S, Li X, Guo L, Luo Z. Experimental research on acetic acid steam reforming over Co–Fe catalysts and subsequent density functional theory studies. *Int J Hydrogen Energy* 2012;37:11122–31.
- [46] Hoang TMC, Geerdink B, Sturm JM, Lefferts L, Seshan K. Steam reforming of acetic acid – a major component in the volatiles formed during gasification of humin. *Appl Catal B Environ* 2015;163:74–82.
- [47] Megia PJ, Cortese M, Ruocco C, Vizcaino AJ, Calles JA, Carrero A, et al. Catalytic behavior of Co-based catalysts in the kinetic study of acetic acid steam reforming. *Ind Eng Chem Res* 2020;59:19531–8.
- [48] Phongprueksathat N, Meeyoo V, Rirksomboon T. Steam reforming of acetic acid for hydrogen production: catalytic performances of Ni and Co supported on Ce_{0.75}Zr_{0.25}O₂ catalysts. *Int J Hydrogen Energy* 2019;44:9359–67.
- [49] Process systems enterprise. gPROMS ModelBuilder. Documentation Release 410. 2015.
- [50] Process Systems Enterprise. Model validation and model-based data analysis. 2019.
- [51] Cheng F, Dupont V, Twigg MV. Direct reduction of nickel catalyst with model bio-compounds. *Appl Catal B Environ* 2017;200:121–32.
- [52] Fuller EN, Schettler PD, Giddings JC. New method for prediction of binary gas-phase diffusion coefficients. *Ind Eng Chem* 2002;58:18–27.
- [53] Arregi A, Lopez G, Amutio M, Barbarias I, Santamaria L, Bilbao J, et al. Kinetic study of the catalytic reforming of biomass pyrolysis volatiles over a commercial Ni/Al₂O₃ catalyst. *Int J Hydrogen Energy* 2018;43:12023–33.
- [54] Barbarias I, Lopez G, Artetxe M, Arregi A, Bilbao J, Olazar M. Kinetic modeling of the catalytic steam reforming of high-density polyethylene pyrolysis volatiles. *Energy Fuels* 2017;31:12645–53.
- [55] Gayubo AG, Valle B, Aramburu B, Montero C, Bilbao J. Kinetic model considering catalyst deactivation for the steam reforming of bio-oil over Ni/La₂O₃-αAl₂O₃. *Chem Eng J* 2018;332:192–204.
- [56] Xu J, Froment GF. Methane steam reforming, methanation and water-gas shift: 1. Intrinsic kinetics. *AIChE* 1989;35:88–96.
- [57] Abbas SZ, Dupont V, Mahmud T. Kinetics study and modelling of steam methane reforming process over a NiO/Al₂O₃ catalyst in an adiabatic packed bed reactor. *Int J Hydrogen Energy* 2017;42:2889–903.
- [58] Aspen Technology Inc. Aspen Plus V.10. Property methods assistant.
- [59] Ayalur Chattanathan S, Adhikari S, Abdoulmoumine N. A review on current status of hydrogen production from bio-oil. *Renew Sustain Energy Rev* 2012;16:2366–72.
- [60] Tian X, Wang S, Zhou J, Xiang Y, Zhang F, Lin B, et al. Simulation and exergetic evaluation of hydrogen production from sorption enhanced and conventional steam reforming of acetic acid. *Int J Hydrogen Energy* 2016;41:21099–108.